TOPOLOGY AND TRANSPORT CHARACTERISTICS IN A TURBULENT TWO-CYLINDER WAKE

M.W. Yiu, Y. Zhou and H. J. Zhang
Department of Mechanical Engineering
The Hong Kong Polytechnic University
Hung Hom, Kowloon, Hong Kong
Email: mmyzhou@polyu.edu.hk

ABSTRACT

This work aims to study experimentally the turbulent flow topology (vortex patterns), heat and momentum transport in the wake of two side-by-side circular cylinders. Spacing T between the cylinder axes was varied from $1.5d$ to $3d$ (d is the cylinder diameter). At T/d = 1.5, the phase-averaged velocity and temperature fields display a single vortex street. The two rows of vortices exhibit a great difference in the maximum vorticity and size and are asymmetrical in the lateral location with respect to the flow centreline. As T/d increases to 3.0, the flow is totally different. Two in-phase streets occur initially. They are less stable, with vortices weakening faster, than the street at T/d = 1.5. By x/d = 40, one street only is identifiable. The momentum and heat transport characteristics of the flow are discussed by examining the coherent and incoherent momentum and heat flux vectors.

INTRODUCTION

Flow around two side-by-side cylinders has received considerable attention in the past (Zdravkovich 1977; Sumner et al. 1999) because of its inherent importance and practical significance in many branches of engineering. The flow behind two side-by-side cylinders depends to a great extent on the ratio T/d. When $T/d < 1.2$, the two cylinders behave like a single structure (Sumner *et al.* 1999; Zhou *et al.* 2000), generating a single vortex street. For $1.2 < T/d < 2.0$, the gap flow between the cylinders is deflected. The deflected gap flow is bi-stable and randomly changed over from one side to another (Ishigai *et al.* 1972; Bearman & Wadcock 1973; Kim & Durbin 1988). As T/d is increased beyond 2, two distinct vortex streets have been observed (Landweber 1942). The two streets are coupled, with a definite phase relationship. Williamson (1985) showed at Reynolds number Re ($\equiv U_\infty d/\nu$, where U_∞ is the free stream velocity and ν is the kinematic viscosity) = 100 – 200 that the two streets may occur in phase or in antiphase. The in-phase streets eventually merged downstream to form a single street, while the in-antiphase streets remained distinct farther downstream.

Most of information obtained on the two-cylinder wake is based on flow visualisation data at a low Reynolds number, thus providing a qualitative description only of the flow. Based on ensemble-averaged LDA measurements, Kolář *et al.* (1997) studied the turbulent near-wake of two side-by-side square cylinders for T/d = 3.0 and Re = 23100. They found that the circulation of inner vortices, i.e. those shed on the side towards the flow centreline, decreased faster than that of outer vortices, which were shed on the free stream side. Their study however did not cover the single vortex street regime ($T/d < 2.0$). Sumner et al. (1999) studied the wake of two and three side-by-side circular cylinders in a range of T/d = 1 ~ 6 for Re = 500 ~ 3000. Their flow visualisation unveil some interesting details of vortex shedding and gap flow between cylinders for a relatively high Re. Using a combination of an X-wire and a cold wire, Zhou *et al.* (2000) measured the velocity and temperature fluctuations at Re = 1800. They observed that the cross-stream distributions of the Reynolds stresses and heat flux vary significantly as T/d reduced from 3.0 to 1.5, implying a different flow topology (the pattern of vortical structures). Although it is by now well known that the number of vortex streets are different for the two flow regimes, many details of the flow topology, especially the temperature field, remain unknown. Therefore, the first objective of the present work is to study the effect of T/d on the topology of the velocity and temperature fields. One may surmise that the momentum and heat transport characteristics of the flow may not be the same as those in a single cylinder wake. The second objective is to understand the manner in which the momentum and heat transport is carried out as T/d varies and compares it with a single cylinder wake.

EXPERIMENTAL DETAILS

Experiments were carried out in a closed circuit wind tunnel with a square cross-section (0.6 m x 0.6 m) of 2.0 m long. The wake was generated by two brass cylinders (d = 12.7mm) arranged side-by-side (Fig. 1). The cylinders were installed horizontally in the mid-plane and spanned the full width of the working section. They were located at 20 cm downstream of the exit plane of the contraction. This resulted in a maximum blockage of about 4.2% and an aspect ratio of 47. The transverse spacing between the cylinders was varied from T/d = 1.5 to 3.0. Both cylinders were electrically heated. The maximum temperature difference between the cylinders

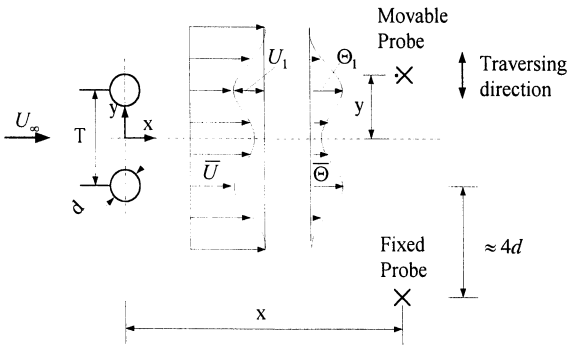

Figure 1 Experimental arrangement.

and the ambient fluid, Θ_1, was approximately 1.0°C. At this level of heating, the temperature can be safely treated as a passive scalar at the three measurement stations, x/d = 10, 20 and 40. Measurements were made at a free-stream velocity U_∞ of 7m/s, or Re = 5800.

A three-wire probe (an X-wire plus a cold wire) was used to measure the velocity fluctuations in the streamwise and lateral directions, u and v, respectively, and the temperature fluctuation, θ. The three-wire probe was traversed across the flow. One X-wire was used in conjunction with the three-wire probe in order to provide a phase reference for the signals from the three-wire probe. The X-wire was fixed at $4d$ below the centre of the lower cylinder. The hot wires were etched from a 5μm diameter Wollaston (Pt-10% Rh) wire to a length of about 1 mm. As for the cold wire, a 1.27μm diameter Wollaston (Pt-10% Rh) wire was etched to a length of about 1.2 mm and a temperature coefficient of 1.69 x 10^{-3} $°C^{-1}$ (Browne & Antonia, 1986) was used. Constant-temperature and constant-current circuits were used for the operation of the hot wires and the cold wire, respectively. An overheat ratio of 1.8 was applied for the X-wire, while a current of 0.1 mA was used in the cold wire. Signals from the circuits were offset, amplified and then digitised using a 16 channel (12bit) A/D board and a personal computer at a sampling frequency $f_{sampling}$ = 3.5kHz per channel. The duration of each record was about 10s.

PHASED-AVERAGED VELOCITY AND TEMPERATURE FIELDS

Vortices shed from a bluff body are characterised with a marked periodicity. In the near or intermediate wake, a small dispersion is expected in the spanwise spacing, lateral location, strength and shape of the vortices. The marked periodicity persists even in the presence of a neighbouring cylinder. The experimental data is therefore phase-averaged. The phase averaging method is similar to that used by Matsumura & Antonia (1993). Interested readers may refer to their paper for more details of this technique. The phase average of an instantaneous quantity B is given by $\tilde{B}_k = \frac{1}{N}\sum_{i=1}^{N} B_{k,i}$, where k represents phase. For convenience, the subscript k will be omitted hereinafter. N is about 600 for T/d =1.5 and 1200 for T/d = ∞ & 3.0 (The single cylinder case is also conveniently referred to as T/d = ∞ in this paper). The variable B can be viewed as the sum of the time mean component $\overline{B}$ and the fluctuation component β. The latter can be further decomposed into the coherent fluctuation $\tilde{\beta} \equiv \langle\beta\rangle$ and a remainder (incoherent fluctuation) β_r, viz., $\beta = \tilde{\beta} + \beta_r$. Also, $<\beta\gamma> = \tilde{\beta}\tilde{\gamma} + <\beta_r\gamma_r>$.

Figures 2 & 3 present the iso-contours of phase-averaged vorticity and corresponding sectional streamlines. In this paper, an asterisk denotes normalisation by either U_∞, Θ_1 and d. This normalisation is used for convenience because the velocity and temperature fields of the present flow are not self-preserving. The phase ϕ, ranging from - 2π to + 2π, can be interpreted in terms of a longitudinal distance; ϕ = 2π corresponds to the average vortex wavelength. To avoid any distortion of the physical space the same scales are used in the ϕ- and y^*-directions in Figs. 2 & 3 and other figures that follow. Vorticity is calculated by $\tilde{\omega} = \frac{\partial(\overline{V}+\tilde{v})}{\partial x} - \frac{\partial(\overline{U}+\tilde{u})}{\partial y} \approx \frac{\Delta\tilde{v}}{\Delta x} - \frac{\Delta(\overline{U}+\tilde{u})}{\Delta y}$, where $\Delta x = -U_c\Delta t = -U_c / f_{sampling}$, U_c is the average convection velocity of vortices, given by the velocity $\overline{U} + \tilde{u}$ at the vortex centre. The vortex

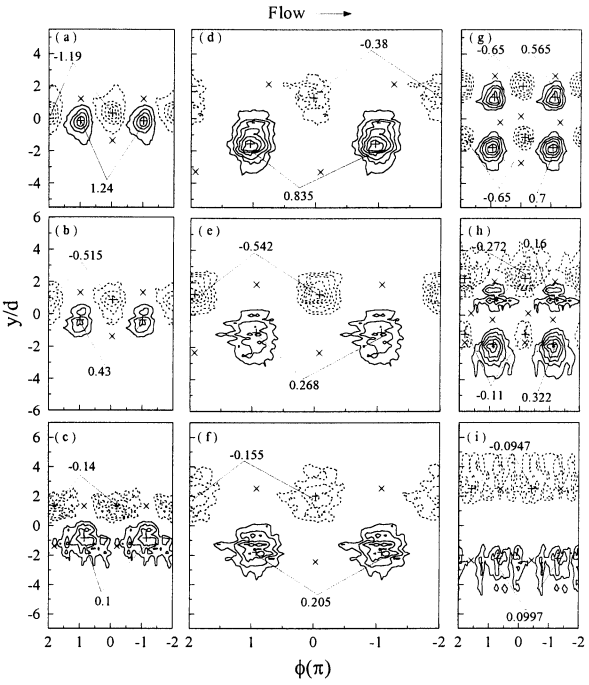

Figure 2 Phase-averaged vorticity contours $\tilde{\omega}^*$. (a-c) T/d = ∞: x/d = 10, contour interval = 0.27; 20, 0.135; 40, 0.03. (d-f) T/d = 1.5: 10, 0.135; 20, 0.081; 40, 0.045. (g-i) T/d = 3.0: 10, 0.135; 20, 0.054; 40, 0.0243.

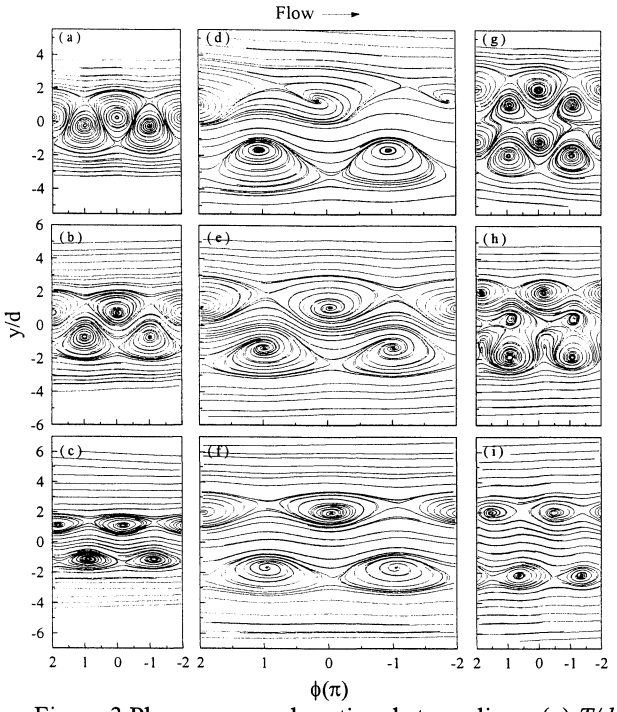

Figure 3 Phase-averaged sectional streamlines: (a) T/d = ∞, x/d = 10; (b) ∞, 20; (c) ∞, 40; (d) 1.5, 10; (e) 1.5, 20; (f) 1.5, 40; (g) 3.0, 10; (h) 3.0, 20; (i) 3.0, 40. The U_c^* values in Table 1 are used in construction of sectional streamlines.

centre is identified with the location of the maximum phase-averaged vorticity $\tilde{\omega}_{max}$, marked by '+' in Fig. 2. The estimate of U_c is given in Table 1. *Upper* and *Lower* in the table stand for the vortices above and below the flow centreline y = 0, respectively. It will be seen that at T/d = 3.0 two vortex streets occur. *Outer* in the table denotes the outer vortices, which are shed from the side of a cylinder nearer to the free stream; *Inner* represents the inner vortices shed from the side of a cylinder close to the flow centreline. The result at T/d = ∞ is in good agreement with Zhou & Antonia (1992)'s measurement, lending credence to the present estimate. For T/d = 3.0, the U_c values are practically the same for the upper and lower row vortices but the outer vortex appears to have a larger U_c than the inner. The difference is probably because the outer row vortices are farther away from the flow centreline. The vortex path, i.e. the most likely lateral distance $y_c^* = y_c/d$ (Table 1) of the vortex from the flow centreline is about 1.9 for the outer vortices and 1.3 for the inner vortices. For the same token, there is a difference in U_c between the upper and lower row vortices for T/d = 1.5; the difference is quite significant at x/d = 10. It should be mentioned that $\tilde{\omega}^*$ impairs as x/d increases. Consequently, the uncertainty arises in the determination of the vortex centre, thus adversely affecting the estimate of U_c. This is particularly evident for the inner vortices and hence their y_c and U_c values for $x/d \geq 20$ are not given in Table 1. The U_c value of the outer vortex is also used to calculate the averaged vortex wavelength, i.e. $U_c T_s = U_c/f_s$.

A single cylinder wake and the two-cylinder wake at T/d = 1.5 display a single vortex street. The street at T/d = 1.5 is however distinctly different from that at T/d = ∞. Firstly, the two rows of vortices have a large lateral spacing. For example, this spacing for T/d = 1.5 is 2.85, 2.28 and 3.8 for x/d = 10, 20 and 40, respectively. The corresponding spacing is only 0.46, 1.60 and 2.58 for T/d =∞. Their wavelength is also greater than that at T/d = ∞. Spectral analysis indicates a single vortex frequency across the wake (this is also true for T/d = 3.0). The corresponding Strouhal number $St = f_s d/U_\infty$ is 0.11, about one half of that (0.21) at T/d = ∞ or 3.0.

Two in-phase vortex streets are seen up to x/d = 20 for

Table 1 Some characteristic properties of vortices

T/d			∞			1.5			3.0		
X/d			10	20	40	10	20	40	10	20	40
y_c^*	Outer	Upper	0.23	0.80	1.29	1.18	1.18	1.89	1.91	2.17	2.44
		Lower				-1.67	-1.10	-1.89	-1.90	-2.01	-2.3
	Inner	Upper							1.29		
		Lower							-1.30		
U_c^*	Outer	Upper	0.86	0.87	0.92	0.77	0.80	0.87	0.83	0.84	0.88
		Lower				0.85	0.81	0.89	0.83	0.84	0.87
	Inner	Upper							0.80		
		Lower							0.80		
$\tilde{\omega}_{max}^*$	Outer	Upper	-1.216	-0.516	-0.151	-0.490	-0.579	-0.184	-0.797	-0.284	-0.098
		Lower	1.267	0.461	0.128	1.025	0.292	0.263	0.835	0.33	0.103
	Inner	Upper							0.707	0.173	
		Lower							-0.727	-0.126	

T/d = 3.0. The inner vortices are weak in terms of $|\tilde{\omega}^*_{max}|$ and small in size, as compared with outer vortices. Kolář et al. (1997) studied the near-wake behind two side-by-side square cylinders and noted a fast decay in inner vortices in the base region.. They employed effective turbulent vorticity flux density vector $\vec{J} = \{J^x, J^y\}$, where

$$J^x = \frac{\partial}{\partial y}\left[\frac{< v_r^2 > - < u_r^2 >}{2}\right] + \frac{\partial}{\partial x} < u_r v_r >, \quad (2a)$$

$$J^y = \frac{\partial}{\partial x}\left[\frac{< v_r^2 > - < u_r^2 >}{2}\right] - \frac{\partial}{\partial y} < u_r v_r >. \quad (2b)$$

As discussed in detail by Hussain (1986) and Kolář et al., the vector may provide a measure of the transport of vorticity. Based on phase-averaged $\vec{J}$, they inferred in the base region that, while an outer vortex interacted primarily with the upstream inner vortex, an inner vortex interacted most vigorously with cross-stream inner vortices, as well as with outer vortices. They suggested that the interaction between the inner vortices shed from the different cylinders was mainly responsible for the fast decay in inner vortices.

The fast decay in inner vortices is also evident in the present data. As a matter of fact, the two streets are less stable than the single street at $T/d = \infty$ or 1.5. At x/d = 10, the ratio of $|\tilde{\omega}^*_{max}|$ of the inner vortex to that of the outer vortex is about 0.83. It drops to 0.50 at x/d = 20. By x/d = 40, vorticity contours (Fig. 2i) show a blank zone in the central region; one street only is identifiable (Fig. 3i).

Using flow visualisation, Williamson (1985) observed that, in a laminar flow, two in-phase laminar streets formed behind two side-by-side cylinders (T/d = 4.0) and further developed into one large-scale single street downstream. He proposed that like-signed vortices in the two streets paired up and formed binary vortices. These binary vortices coalesced to form the single street. Such a development was however not observed in Sumner *et al.* (1999)'s PIV data (Re = 500 ~ 3000). The $\tilde{\omega}^*$ contours (Fig. 2) and sectional streamlines (Fig. 3) also do not suggest the coalescence of binary vortices to be a major mechanism behind the present observation in the turbulent wake.

The inner vortices appear squashed, each surrounded by four oppositely signed vortices. One may surmise that the faster decay in vorticity level results from interaction between the oppositely signed vortices. This is indeed supported by effective turbulent vorticity flux density vectors $\vec{J}$ (Fig. 4). The vector length in Fig. 4 is proportional to the magnitude of $\vec{J}$, thus representing the strength of vorticity flux or exchange. The outermost vorticity contour in Fig. 2, which corresponds to the lowest level displaying a clear pattern of vortices, is also plotted in Fig. 4 to indicate approximately the boundary of individual vortices. The vortex centres and saddle points, identified from sectional streamlines (Fig. 3), are marked by '+' and '×', respectively, in this figure and those following for the convenience of data interpretation. For $T/d = \infty$, the vorticity flux appear moving from one vortex, such as the one at $\phi = 0$, towards the adjacent ones of opposite sign; the vectors of generally intermediate length cross the vorticity contour both upstream and downstream of the vortices, indicating an exchange between counter-rotating vortices. This is not so evident for T/d = 1.5, suggesting a relatively weak interaction between oppositely signed vortices probably because of a large spacing both longitudinally and laterally. The observation is in fact reconcilable with the persistence of vortices for T/d = 1.5. The present result at T/d = 3.0 is however not quite the same as that inferred by Kolář and his co-workers. At this T/d, relatively long vectors (Fig. 4c) cross the contour of the inner vortex, e.g. at $\phi = 0$. Part of them move towards both upstream and downstream adjacent outer vortices and part of them cross the flow centreline, suggesting that the inner vortex exchanges vorticity with both outer vortices shed from the same cylinder and cross-stream inner vortices shed from the different cylinder. However, judging from the vectors crossing the flow centreline (most of which appear originated from the inner vortices, though not exclusively), the latter exchange appear comparatively weak, probably due to a relatively large spacing between the inner vortices shed from different cylinders (Fig. 4c). But nonetheless weak, this exchange would cause additional

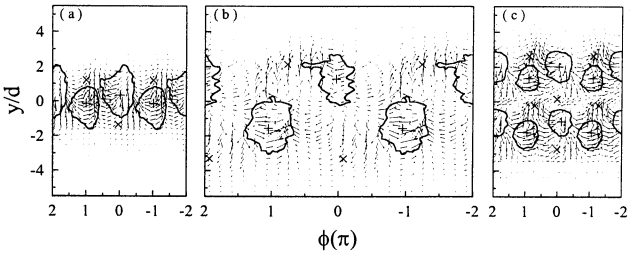

Figure 4 Effective vorticity flux density vectors $\tilde{J}^*$ at x/d = 10. (a) $T/d = \infty$, (b) 1.5, (c) 3.0. Centre and saddles are denoted by "+" and "×".

cancellation in vorticity associated with the inner vortex. On the other hand, the outer vortices appear interacting only with the inner vortices shed from the same cylinder.

There is a close similarity between the $\overline{\Theta}+\tilde{\theta}$ (Fig. 5) and $\tilde{\omega}$ contours at x/d = 10, suggesting an association of heat with the large-scale vorticity concentration. The similarity disappears at x/d = 20 for T/d = 3.0 and at x/d = 40 for $T/d = \infty$. It is evident that higher the maximum vorticity level of a vortex, better the coincidence between the vortex and higher isotherms.

MOMENTUM AND HEAT TRANSPORT

Insight can be gained into the momentum and heat transport characteristics of the flow by examining the

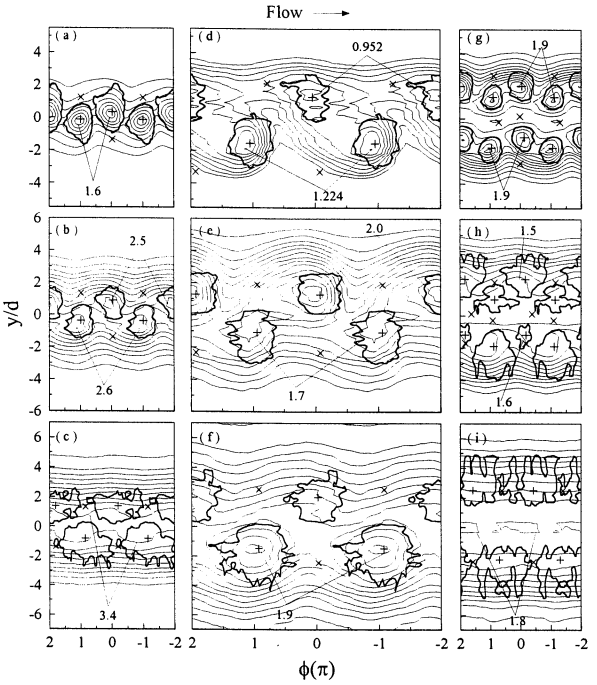

Figure 5 Phase-averaged temperature contours $\overline{\Theta}^* + \tilde{\theta}^*$. (a-c) $T/d = \infty$: $x/d = 10$, contour interval = 0.2; 20, 0.1; 40, 0.1. (d-f) $T/d = 1.5$: 10, 0.136; 20, 0.1; 40, 0.1. (g-i) $T/d = 3.0$: 10, 0.1; 20, 0.1; 40, 0.1. The thicker solid line denotes the outermost vorticity contours in Figure 2.

coherent heat flux vector $\tilde{\boldsymbol{q}} = (\tilde{u}\tilde{\theta}, \tilde{v}\tilde{\theta})$ (Figs. 6d~f) and the incoherent heat flux vector $\tilde{\boldsymbol{q}}_r = (< u_r^*\theta_r^* >, < v_r^*\theta_r^* >)$ (Figs. 6g~i), along with the velocity vector $\boldsymbol{V} - \boldsymbol{V}_c = (\overline{U} + \tilde{u} - U_c, \tilde{v})$ (Figs. 6a~c). The velocity vectors are viewed in a reference frame translating at U_c.

At T/d = ∞, the coherent heat flux vectors within vortices are generally aligned with the velocity vectors, suggesting that the coherent motion does not contribute to the net transport of heat out of vortices. On the other hand, the incoherent heat flux vectors point upstream, responsible mostly for the net heat transport out of vortices.

The two-cylinder case is not quite the same. When T/d is small, such as 1.5, one staggered (perhaps predominantly) vortex street is formed. One row of vortices is substantially weaker in the coherent motion than the other. Their difference in term of the maximum vorticity is a factor of about 2 at x/d = 10 (Table 1). There is also a considerable difference in their sizes (Fig. 2d). The coherent heat flux vectors associated with the lower row vortex, which has a strong coherent motion, exhibit a behaviour similar to their counterpart at $T/d = \infty$, but those associated with the upper row vortex are directed towards the downstream vortex of the opposite sign. The observation is reasonable. Under the effect of the vortical motion, albeit weak, warm fluid ($\theta > 0$) downstream of the upper row vortex centre goes down ($v < 0$). Meanwhile, the negative $\tilde{u}$ component associated with this vortex is suppressed, the rotation of the coherent motion being thus weakened, presumably due to the possible effect of the deflected gap flow. The warm fluid is therefore associated with the positive $\tilde{u}$, giving rise to the positive $\tilde{u}\tilde{\theta}$, whose contours are stretched towards the cross-stream vortex downstream (not shown). The incoherent heat flux vector $\tilde{q}_r$ at $T/d = 1.5$ (Fig. 6h) is generally directed upstream of the vortex centre, indicating a transfer of heat out of vortices.

As the spacing between the cylinders increases, say at $T/d = 3.0$, the flow topology is totally different; two predominantly in-phase vortex streets occur. Vortices in each street are spatially again in the staggered arrangement. The outer vortices have a strong coherent motion, relatively to the inner vortices. Since the two streets are arranged anti-symmetrically about the flow centreline, it is sufficient to examine one street only for the study of the flow. We will focus on the one above the centreline. The coherent heat flux appears

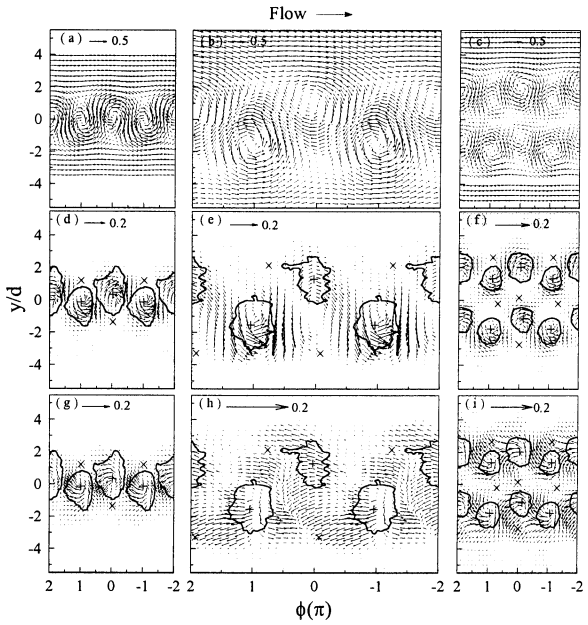

Figure 6 Phase-averaged coherent velocity vectors $\tilde{V}^*$ and heat flux vectors $\tilde{q}^*$ and incoherent heat flux vectors $\tilde{q}_r^*$ at $x/d = 10$. (a-c) $T/d = \infty$; (d-f) 1.5; (g-i) 3.0.

circulating within the outer vortex, implying a small net transport of heat out of the vortex. But $\tilde{\boldsymbol{q}}$ associated with the inner vortices is seen crossing the vorticity contour, pointing partly towards the free stream and partly towards the downstream outer vortex shed from the same cylinder.

At T/d = 3.0, $\tilde{\boldsymbol{q}}_r$ points upstream within the vortex, as $T/d = 1.5$ or ∞. However, upstream of the inner vortex, in particular outside the vorticity contour, $\tilde{\boldsymbol{q}}_r$ is directed towards the free stream.

CONCLUSIONS

The turbulent wake behind two side-by-side circular cylinders has been investigated using a phase-averaging technique. It has been found that the flow pattern, heat and momentum transport depend on the cylinder-to-cylinder centre spacing. The following conclusions can be drawn.

At T/d = 1.5, a single vortex street is seen throughout the range of x/d = 10 ~ 40. The vortex street is the most stable among the three T/d values. The vortices decay relatively slow. The longitudinal and lateral spacing between vortices is larger at T/d = 1.5. The large spacing implies a weak interaction between vortical motions, probably contributing to the relatively long life span of the vortices and hence the stability of the vortex street. The two rows of vortices behave quite differently. Their convection velocities are not the same at x/d = 10 probably because of an asymmetrical spatial arrangement about the flow centreline. One row of vortices is significantly weaker in strength than the other. The deflected gap flow, discernible from the phase-averaged sectional streamlines, may play an important role in leading to the difference in strength. It could act to suppress the rotational motion of vortices towards which the gap flow is deflected, thus weakening the affected vortices.

As T/d increases to 3.0, the phase-averaged velocity field displays two in-phase vortex streets of the same vortex frequency. The two streets interact vigorously and are unstable, as compared with the cases of T/d = ∞ and 1.5. The vortices decay fast, especially the inner ones that are shed from the side of a cylinder close to the flow centreline. By x/d = 40, the inner vortex completely disappears and one street only is discernible. An interpretation is proposed for the present observation of a turbulent flow. While an outer vortex largely interacts only with adjacent oppositely signed inner vortices, an inner vortex interacts with the cross-stream inner vortices as well as with adjacent outer vortices. As a result, vorticity associated with the inner vortex is annihilated quickly, leading to the early disappearance of inner vortices and formation of a single street.

The spacing between cylinders does have a significant effect on the heat and momentum transport characteristics. It is found that the interaction between the vortex streets at T/d = 3.0 hastens, to a great extent, the transport of heat out of vortices. The inner vortices loose heat even faster than the outer vortices, contributing negligibly to the lateral heat transport. As T/d reduces to 1.5, The coherent heat flux vectors associated with the vortex of greater strength exhibit a behaviour similar to their counterpart at T/d = ∞, the coherent heat flux vectors within vortices are generally aligned with the velocity vectors. But those associated with the vortex of weaker strength are directed towards the downstream vortex of the opposite sign.

REFERENCES

Bearman, P. W. and Wadcock, A. J., 1973, *J. Fluid Mech.*, Vol. 61, pp. 499-511.

Browne, L.W.B. and Antonia, R.A., 1986, *Phys. Fluids,* Vol. 29, pp. 709-713.

Cantwell, B. and Coles, D., 1983, *J. Fluid Mech.,* Vol. 136, pp. 321-374.

Ishigai, S., Nishikawa, E., Nishmura, K. and Cho, K., 1972, *Bull. JSME,* Vol. 15, pp949-956.

Kim, H.J. and Durbin, P.A., 1988, *J. Fluid Mech.,* Vol. 196, pp. 431-448.

Kolář, V., Lyn, D.A. and Rodi, W., 1997, *J. Fluid Mech.,* Vol. 346, pp. 201-237.

Landweber, L., 1942, "Flow about a pair of adjacent, parallel cylinders normal to a stream", D. W. Taylor Model Basin, Department of the Navy, Report 485, Washington, D.C.

Matsumura, M. and Antonia, A., 1993, *J. Fluid Mech.,* Vol. 250, pp. 651-668.

Roshko, A., 1954, "On the drag and shedding frequency of two-dimensional bluff bodies", *NACA TN,* p3169.

Sumner, D., Wong, S.S.T., Price, S.J. and Païdoussis, M.P., 1999, *J. Fluids Structures,* Vol. 13, pp. 309-338.

Williamson, C. H. K., 1985, *J. Fluid Mech.,* Vol. 159, pp. 1-18.

Zdravkovich, M. M., 1977, ASME *J. Fluids Engng.,* Vol. 99, pp. 618-633.

Zhou, Y. and Antonia, R. A., 1992, *Expts. Fluids,* Vol. 13, pp. 63-70.

Zhou, Y., So, R. M. C., Wang, Z. J. and Jin, W., 2001, *J. Fluid Mech.* (accepted).

Zhou, Y., So, R. M. C., Liu, M. H. and Zhang, H. J., 2000, *Int. J. Heat Fluid Flow,* Vol. 12, pp. 125-133.